ELSEVIER

Catalysis Today 44 (1998) 151–163

CATALYSIS TODAY

Dynamic and kinetic modeling of isotopic transient responses for CO insertion on Rh and Mn–Rh catalysts

Mark A. Brundage[1], Steven S.C. Chuang[*], Scott A. Hedrick

Department of Chemical Engineering, The University of Akron, Akron, OH 44325-3906, USA

Abstract

Isotopic transient tracer techniques have been employed to study heterogeneous hydroformylation on Rh/SiO_2 and $Mn–Rh/SiO_2$. Pulse injection of D_2 and ^{13}CO allowed tracing of the deuterium and CO incorporation pathway into the aldehyde product. The d_1- and d_2-propionaldehyde responses showed a double-peak, or two-hump, response to the D_2 pulse, while $C_2H_5\,^{13}CHO$ showed a single-hump response to the ^{13}CO pulse. Analysis of the product responses to the D_2 pulse in $CO/H_2/C_2H_4$ and $CO/H_2/C_2H_4/C_2H_5CHO$ suggests that the first hump of the d_1- and d_2-propionaldehyde responses was due to rapid H/D exchange with adsorbed propionaldehyde via enol intermediates. The decay of the second hump was due to reaction of adsorbed acyl with spillover hydrogen/deuterium. The $C_2H_5\,^{13}CHO$ response was due to CO insertion followed by acyl hydrogenation. Compartment modeling of the product responses from the ^{13}CO and D_2 pulse inputs allowed determination of residence times of adsorbed intermediates, surface coverages of adsorbed intermediates, and the elementary rate constants for acyl hydrogenation and CO insertion. Elementary rate constants for acyl hydrogenation determined from this study were consistent with the value calculated by transition state theory (TST). The addition of Mn promoter to Rh/SiO_2 increased coverages of $^*CO$, $^*C_2H_5$, and $^*C_2H_5CO$ and shifted the rate-limiting step for propionaldehyde formation. Acyl hydrogenation is the rate-limiting step on Rh/SiO_2 while CO insertion and acyl hydrogenation are both kinetically significant on $Mn–Rh/SiO_2$.

Keywords: Reaction dynamics; Kinetic modeling; Isotope; Transient response; Ethylene; ^{13}CO; Rhodium; CO insertion; Hydroformylation; Deuterium; Propionaldehyde; Hydrogenation; Syngas

1. Introduction

The stimulus–response technique has widely been used as an experimental method to study various systems in science and engineering [1]. This technique involves imposing a disturbance to the system and then monitoring the corresponding transient response. Stimuli that can be utilized to impose a disturbance to a system include the following: impulse, pulse, step, ramp, parabolic, and frequency input (sinusoidal) [1–5]. In theory, the transient responses to these various stimuli should give the same information for a given system. In practice, the types and magnitudes of the stimuli are chosen based on the nature of the system.

This stimulus–response technique is extensively utilized in reaction engineering to determine the flow pattern of reactors and reactor models. A step or pulse trace is the most often utilized stimulus due to the ease of experimentation and analysis. The tracer response has been used to determine the residence time dis-

*Corresponding author. Tel.: 00 1 330 972 6993; fax: 00 1 330 972 5856; e-mail: schuang@uakron.edu

[1]Present address: General Motors, Rochester, NY.

0920-5861/98/$32.00
PII S0920-5861(98)00186-2

tribution (RTD) of the tracer in the reactor. The RTD of the tracer can be defined by its first moment (i.e., average residence time (τ)) and its second moment (i.e., variance, (σ)) [1,6,7]. RTD allows determination of the reactor model suitability and the values of its parameters.

The stimulus–response technique has been applied to heterogeneous catalytic reactions with changes in the feed concentration and temperature as the stimuli [8–10]. Due to the strong dependence of reaction rate and adsorbate concentration on the reaction conditions, the perturbation in reaction conditions may change the chemical environment of the catalyst surface, the adsorbate concentration, and the rate of product formation. To minimize the disturbance to the catalyst surface state, the steady-state isotopic transient kinetic analysis (SSITKA) technique has been developed to study CO hydrogenation [11,12], ammonia synthesis [13], CO oxidation [14], benzene hydrogenation [15], and many other related reactions [16]. The uniqueness of this technique is the use of an isotope-labeled reactant having similar chemical properties as the non-labeled reactant. Replacement of non-labeled reactant flow by labeled reactant flow at one to one ratio minimizes the disturbance to the chemical environment of adsorbate and catalyst surface from the flow system. The isotope effect on adsorption, surface reaction, and desorption decreases as the mass ratio of labeled tracer to its non-labeled counterpart approaches one [17].

SSITKA studies have been conducted by injection of an isotope tracer by pulse and step mode. We have utilized the pulse isotope tracer technique to study hydroformylation over Rh/SiO_2 and $Mn–Rh/SiO_2$ [18–20]. Ethylene hydroformylation involves half-hydrogenation of adsorbed ethylene, the insertion of adsorbed CO into adsorbed ethyl, and hydrogenation of adsorbed acyl species to form propionaldehyde as shown in the reaction steps listed in Table 1. Use of ^{13}CO as a labeled tracer allows tracing the pathway involved with adsorbed CO; use of D_2 as a labeled tracer allows tracing the pathway involved with hydrogen. Pulse injection of these tracers produced transient responses which allow for determination of kinetic parameters for the postulated elementary steps.

This paper reports results of compartment modeling of the transient responses to the ^{13}CO and D_2 pulses during ethylene hydroformylation over Rh/SiO_2 and $Mn–Rh/SiO_2$. The pathway leading to the transient propionaldehyde responses was determined with results of the D_2 pulse into the $C_2H_5CHO/CO/H_2/C_2H_4$ stream. Modeling of the transient responses produced the values for the rate constants and coverage of active adsorbates which gives insight into the role of Mn promoter in the catalytic cycle of propionaldehyde formation.

Table 1
Ethylene hydroformylation mechanism

Step 1	$H_2+2* \leftrightarrow 2*H$	Hydrogen adsorption
Step 2	$CO+* \leftrightarrow *CO$	CO adsorption
Step 3	$C_2H_4+* \leftrightarrow *C_2H_4$	Ethylene adsorption
Step 4	$*C_2H_4+*H \leftrightarrow *C_2H_5+*$	Partial ethylene hydrogenation
Step 5	$*C_2H_5+*CO \leftrightarrow *C_2H_5CO+*$	CO insertion
Step 6	$*C_2H_5CO+*H \leftrightarrow C_2H_5CHO+2*$	Acyl hydrogenation
Step 7	$*C_2H_5+*H \leftrightarrow C_2H_6+2*$	Alkyl hydrogenation

*Indicates active site.

2. Experimental

2.1. Reaction studies

Fig. 1 illustrates the experimental apparatus used in this study. The catalyst powder (either Rh/SiO_2 or $Mn–Rh/SiO_2$) was pressed into self-supporting disks. The IR reactor cell, which has been reported elsewhere [21], acts as a differential reactor which provides the initial rates for the forward reaction.

The reactant mixture consisted of $CO/H_2/C_2H_4/He$ at a ratio of 1/1/1/1 for a total flow rate of 120 $cm^3\ min^{-1}$ at 513 K and 0.1 MPa. Upon reaching steady-state of reactions for 15 min, the steady-state gaseous reactant and product concentrations were determined by an HP-5890A gas chromatograph (GC) equipped with a flame ionization detector (FID). Following the GC sample, a 6-port valve was used to introduce: (i) a 10 cm^3 pulse of ^{13}CO into the steady-state ^{12}CO flow while maintaining H_2 and C_2H_4 flows at steady-state and (ii) a 10 cm^3 pulse of D_2 into the steady-state H_2 flow while maintaining CO and C_2H_4 flows at steady-state. During the pulse switch, the transient responses of the adsorbates on the catalyst surface were monitored by the IR spectrometer. The transient responses of the gaseous reactants and products from the IR cell were recorded by a

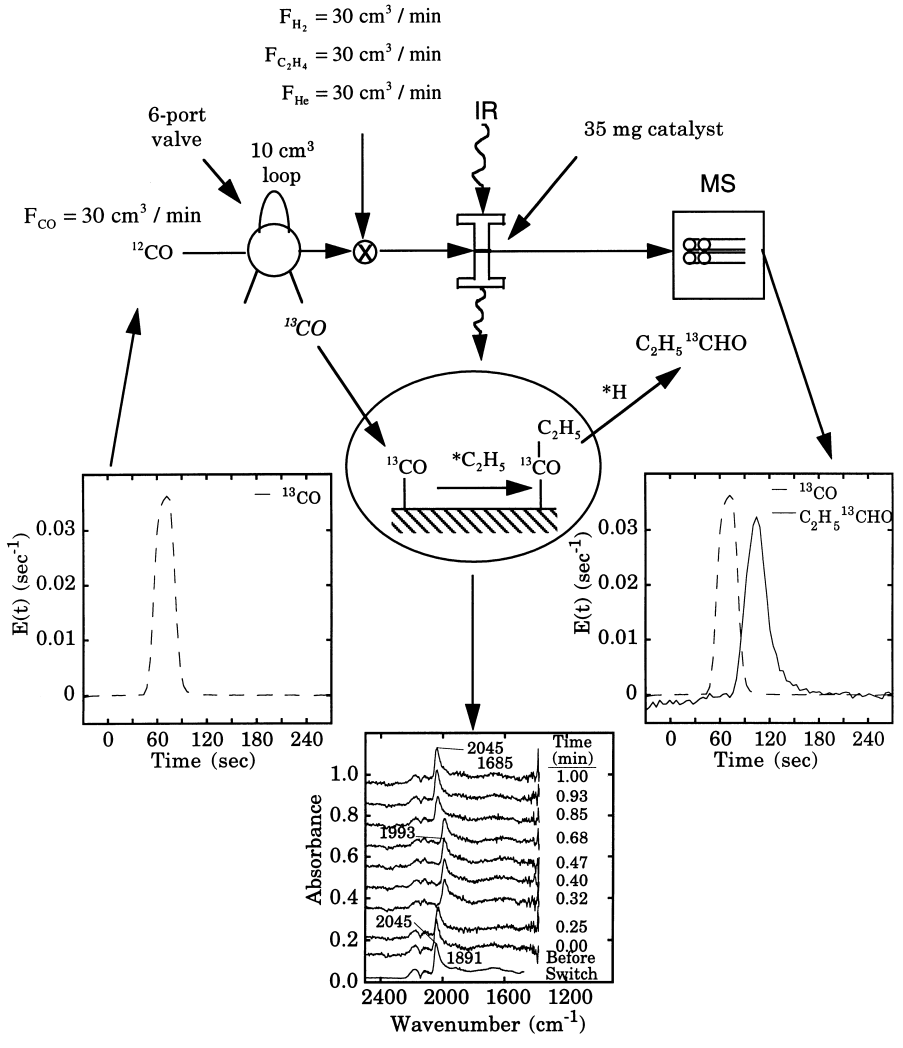

Fig. 1. Experimental approach.

Balzers QMG 112 mass spectrometer (MS) that was interfaced to a computer allowing the simultaneous measurement of 8 m/e (i.e. amu) as a function of time.

3. Results and discussion

3.1. Response to ^{13}CO and D_2 pulses on Rh/SiO_2 and $Mn–Rh/SiO_2$

Experimental responses to the ^{13}CO pulse have been separately reported elsewhere [18,19,22,28] and are reproduced in Fig. 2(a) and Fig. 3(a) for comparison and modeling purposes. The transient responses are normalized to an $E(t)$ curve, where $E(t)$ is defined as

$$E(t) = \frac{C(t)}{\int_0^\infty C(t)\,\mathrm{d}t}, \tag{1}$$

where $C(t)$ is the concentration of the species during the pulse [18]. Fig. 2(a) shows that at time=0, the pulse injection of ^{13}CO was made. Contained in the ^{12}CO stream is 2% Ar, which does not interact with the catalyst surface and is utilized as a tracer to determine

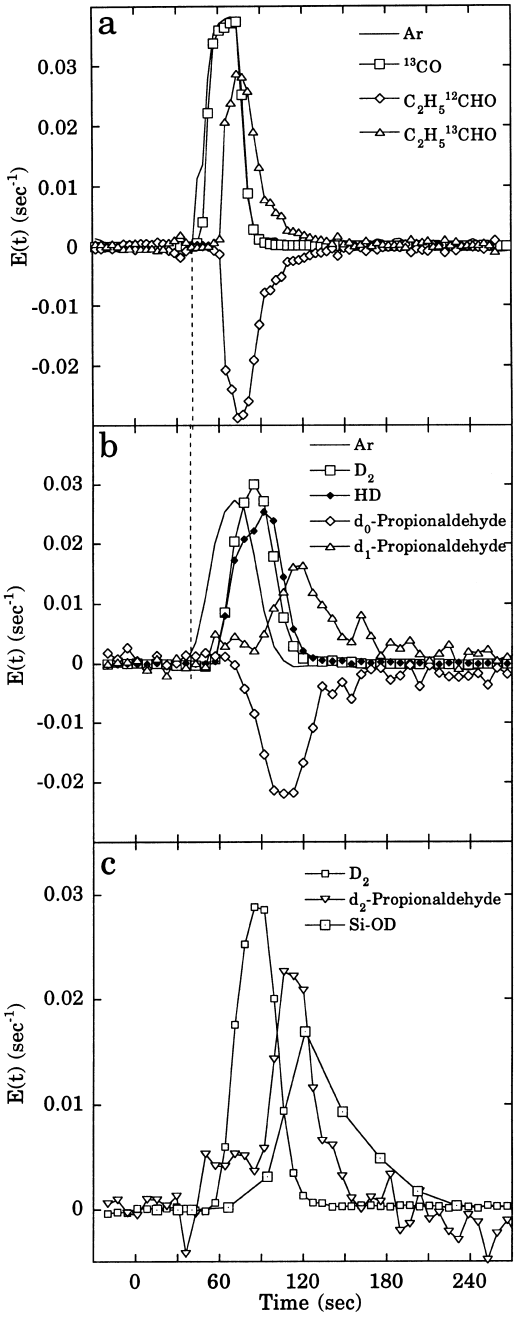

Fig. 2. (a) Transient responses of Ar, ^{13}CO, and $C_2H_5\,^{13}CHO$ to a ^{13}CO pulse into a ^{12}CO stream over Rh/SiO_2, (b) transient responses of Ar, H_2, D_2, HD, d_0-propionaldehyde, and d_1-propionaldehyde to a D_2 pulse into a H_2 stream, and (c) Transient responses of d_2-propionaldehyde and Si-OD to a D_2 pulse into a H_2 stream. (Note that the Ar responses shown are the mirror images of the true responses.)

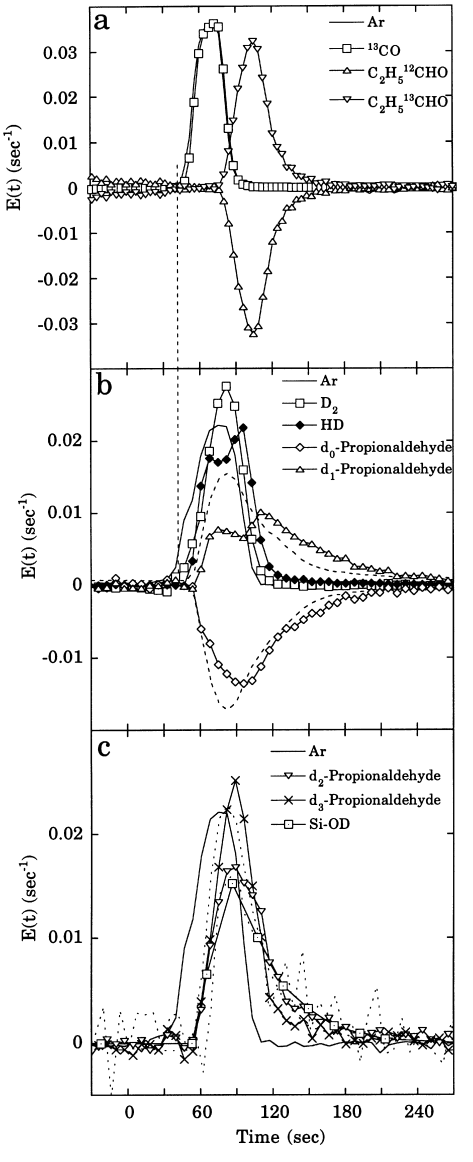

Fig. 3. (a) Transient responses of Ar, ^{13}CO, and $C_2H_5\,^{13}CHO$ to a ^{13}CO pulse into a ^{12}CO stream over $Mn–Rh/SiO_2$. (Reprinted from Applied Catalysis A: General, 151, S.S.C. Chuang, M.A. Brundage, and M.W. Balakos, Mechanistic Study in Catalysis Using Dynamic and Isotopic Transient Infrared Spectroscopy: CO/H_2/C_2H_4 Reaction on $Mn–Rh/SiO_2$, p. 333–354, Copyright 1997, with kind permission of Elsevier Science – NL, Sara Burgerhartstraat 25, 1055 KV Amsterdam, Netherlands), (b) transient responses of Ar, H_2, D_2, HD, d_0-propionaldehyde, and d_1-propionaldehyde to a D_2 pulse into a H_2 stream, and (c) transient responses of d_2-propionaldehyde, d_3-propionaldehyde, and Si-OD to a D_2 pulse into a H_2 stream. (Note that the Ar responses shown are the mirror images of the true responses.)

the flow patterns in the reactor and piping. The lag of the C_2H_5 ^{13}CHO behind the ^{13}CO response is a result of adsorbed ^{13}CO participating in CO insertion to form an adsorbed ^{13}C acyl species which is then hydrogenated to form C_2H_5 ^{13}CHO. Comparing the ^{13}CO pulse product responses in Fig. 2(a) and Fig. 3(a) show that the Mn promoter increased the delay of C_2H_5 ^{13}CHO response. The IR results, which have been presented elsewhere [18], show a rapid exchange between the gaseous CO and adsorbed CO.

The deuterated propionaldehyde responses to a D_2 pulse on Rh/SiO_2 and $Mn–Rh/SiO_2$ have recently been studied [20] and are shown in Fig. 2(b) and (c) and Fig. 3(b) and (c). The H_2 stream contains 2% Ar. The HD, d_0-, d_1-, d_2-, and d_3-propionaldehyde products show distinctly different responses. The two-hump response for d_1- and d_2-propionaldehyde is a result of different isomers (i.e., C_2H_5CDO and C_2H_4DCHO for d_1-propionaldehyde) produced from different deuteration pathways [23]. To compare the lead/lag relationship, Ar for both the ^{13}CO and D_2 pulses are synchronized. Due to a slight difference in the flow lines, flow rates, and the amount of catalyst for these two experiments, the Ar responses for the ^{13}CO and D_2 experiments do not perfectly match.

Fig. 2(b) and (c) and Fig. 3(b) and (c) show that both catalysts produced two-hump responses for d_1- and d_2-propionaldehyde, and a single hump response for d_3-propionaldehyde. Assuming all the deuterated propionaldehyde responses have the same response factor, the deuterated propionaldehyde response areas can be utilized to determine the relative amount produced. Table 2 provides the deuterium distribution in the propionaldehyde product between the two-hump responses. The deuterium distribution in the first-hump propionaldehyde responses go through a maximum at d_3-propionaldehyde for the Rh/SiO_2 catalyst and d_2-propionaldehyde for the $Mn–Rh/SiO_2$ catalyst. In the second hump only d_1-propionaldehyde and d_2-propionaldehyde are observed, with both catalysts having a similar d_1/d_2 ratio of about 2. For the Rh/SiO_2 catalyst, the majority of the deuterium is incorporated in the second hump while for the $Mn–Rh/SiO_2$ catalyst, there is almost an equal distribution between the two-hump responses.

The peak of the second-hump of the d_1- and d_2-propionaldehyde responses aligns with the C_2H_5 ^{13}CHO response for the $Mn–Rh/SiO_2$ catalyst, indicating they may have the same rate limiting steps. For both catalysts, the decay of the second hump d_1- and d_2-propionaldehyde responses are delayed behind the C_2H_5 ^{13}CHO and are parallel to Si-OD (spillover deuterium) response suggesting that the decay portion of the second hump is due to reaction with Si-OD [23].

3.2. Assignment of two-hump response

The first-hump of the d_1- and d_2-propionaldehyde responses coincided with the d_3-propionaldehyde response, shown in Fig. 3, suggesting rapid H/D exchange on either the adsorbed acyl species or propionaldehyde species. To determine the extent of deuterium exchange with propionaldehyde, a D_2 pulse experiment with propionaldehyde present was conducted. H_2, CO, C_2H_4, C_2H_5CHO and He at a 1/1/1/0.01/1 ratio were flown at a total flow rate of 120 cm^3/min over $Mn–Rh/SiO_2$ catalyst at 513 K. A 10 cm^3 pulse of D_2 into the steady-state H_2 stream was then introduced and the deuterated propionaldehyde responses were monitored as shown in Fig. 4.

Table 2
Deuterium distribution in propionaldehyde

	Rh/SiO_2[a]		$Mn–Rh/SiO_2$[a,b]		$Mn–Rh/SiO_2$[c]
	First hump (%)	Second hump (%)	First hump (%)	Second hump (%)	First hump (%)
d_1	3.9	47.6	12.8	33.5	29.1
d_2	5.7	26.7	13.9	15.5	32.5
d_3	15.6	—	13.8	—	38.4
d_4	0.4	—	5.7	—	—
d_5	—	—	4.9	—	—

[a] D_2 pulse into H_2 with CO/C_2H_4.
[b] From [22].
[c] D_2 pulse into H_2 with $CO/C_2H_4/C_2H_5CHO$.

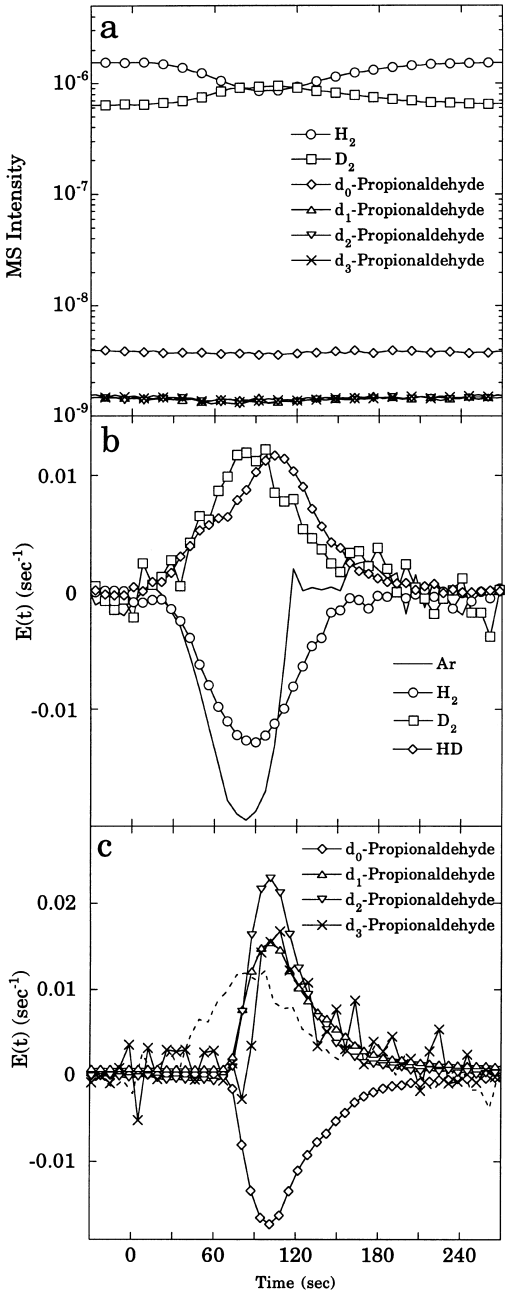

Fig. 4. (a) Transient responses of H_2, D_2, d_0-, d_1-, d_2-, and d_3-propionaldehyde to a D_2 pulse into H_2 with $CO/C_2H_4/C_2H_5CHO$/He at 513 K and 0.1 MPa in the absence of a catalyst, (b) transient responses of Ar, H_2, D_2, and HD to a D_2 pulse into H_2 with $CO/C_2H_4/C_2H_5CHO$/He at 513 K and 0.1 MPa on Mn–Rh/SiO_2, and (c) transient responses of d_0-, d_1-, d_2-, and d_3-propionaldehyde to a D_2 pulse into H_2 with $CO/C_2H_4/C_2H_5CHO$/He at 513 K and 0.1 MPa on Mn–Rh/SiO_2.

Fig. 4(a) shows the response to a D_2 pulse into H_2 in $CO/C_2H_4/C_2H_5CHO$/He in the absence of catalyst to determine the contribution from gas phase reaction to form deuterated propionaldehyde product. The only species that showed a response are the D_2 and H_2, while the deuterated propionaldehyde responses were unchanged during the D_2 pulse, indicating the reaction between D_2 and C_2H_5CHO did not occur in the absence of catalyst. Fig. 4(b) shows the normalized Ar, H_2, HD, and D_2 responses to the experiment over the catalyst. The D_2 shows a positive response and the H_2 shows a negative response as expected. The HD response shows a two-hump positive response that has previously been observed and reported for this catalyst [20]. The deuterated propionaldehyde responses are shown in Fig. 4(c). The negative d_0-propionaldehyde response indicates the consumption of d_0-propionaldehyde from the reaction of d_0-propionaldehyde with D_2. The positive d_1-, d_2-, and d_3-propionaldehyde responses are a result of deuterium incorporation into propionaldehyde. The d_2- and d_3-propionaldehyde may be formed via keto-enol tautomerism and the reaction of enol intermediates with $^*D$ [22]. Similar tautomerisms and intermediates have been suggested for higher alcohol formation from syngas [24,25].

Table 2 contains the deuterium distribution in the deuterated propionaldehyde product. This D_2 pulse into propionaldehyde experimental results show a similar deuterium distribution to the first hump of the D_2 pulse into H_2 with CO/C_2H_4 over Mn–Rh/SiO_2. High deuterium content in d_2- and d_3-propionaldehyde in Table 2 and overlapping of d_1-, d_2-, and d_3-propionaldehyde responses in Fig. 4(c) indicate that H/D exchange to incorporate deuterium to propionaldehyde is a rapid process. Plotting of the deuterated propionaldehyde responses from the D_2 pulse into $CO/H_2/C_2H_4/C_2H_5CHO$ is shown as the dashed lines in Fig. 3(b) and (c) and gives an $E(t)$ curve similar to the first-hump response.

4. Response to a H_2 pulse on Mn–Rh/SiO_2

To confirm that the decay of the d_1-propionaldehyde responses are due to reaction with Si-OD, a H_2 pulse into D_2 experiment was undertaken and is shown in Fig. 5. Fig. 5(a) and (b) show selected deuterated

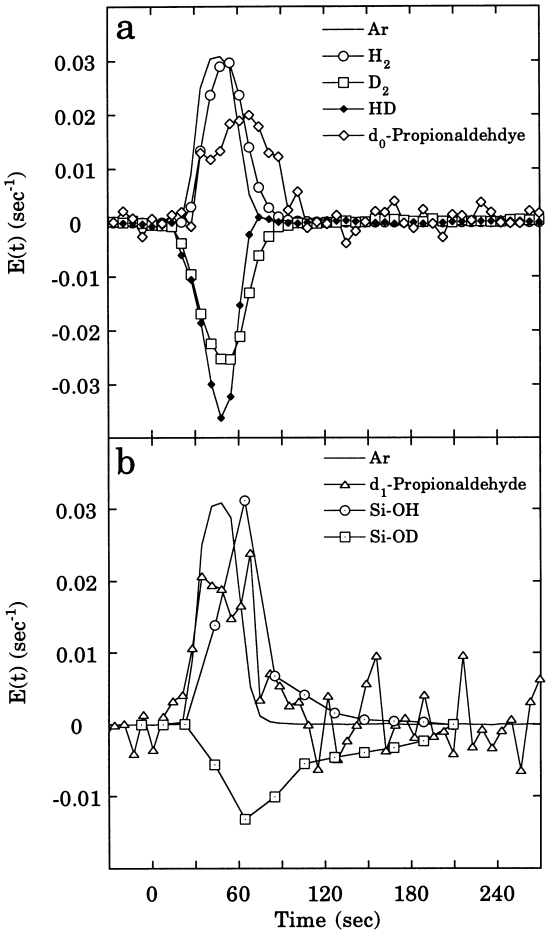

Fig. 5. (a) Transient responses of Ar, H_2, D_2, HD, and d_0-propionaldehyde to a H_2 pulse into a D_2 stream, and (b) transient responses of d_1-propionaldehyde and Si–OH to a H_2 pulse into a D_2 stream.

product responses to a 10 cm^3 H_2 pulse into the steady-state flow of D_2 with steady-state CO and C_2H_4 flow on Mn–Rh/SiO_2 at the same conditions. The HD response shows a negative response because of the removal of the deuterium source. Similarly, during the D_2 pulse, the d_0-propionaldehyde response is observed immediately after the H_2 pulse is introduced. The d_0- and d_1-propionaldehyde responses both show a two-hump response. The first hump of the d_0-propionaldehyde response is suggested to be due to the sudden increase in the concentration of d_0-acyl species and its hydrogenation, while the second hump is due to the H/D exchange on the adsorbed alkyl species ($C_2H_xD_{5-x} \rightarrow C_2H_5$) which then undergoes CO insertion and hydrogenation by Si–OH.

Table 3
Deuterated ethylene and ethane deuterium distributions during steady-state CO/D_2/C_2H_4 reaction at 513 K

	Rh/SiO_2		Mn–Rh/SiO_2	
	Ethylene (%)	Ethane (%)	Ethylene (%)	Ethane (%)
d_0	—	3.0	—	2.6
d_1	88.2	0.9	72.8	1.2
d_2	6.7	0.4	17.5	0.9
d_3	0.6	0.3	3.8	0.4
d_4	—	—	0.8	—

The possible presence of d_0-acyl is supported by the formation of d_0-ethane as a major hydrogenation product during steady-state CO/D_2/C_2H_4 as shown in Table 3. Both d_0-ethane and d_0-acyl share a common intermediate, $^*C_2H_5$, which can be produced from a reversible partial hydrogenation of olefin following the classical Horiuti–Polanyi mechanism [26]. Due to the small amount of catalyst used for this experiment, the higher deuterated propionaldehyde responses are noisy and thus a good deuterium distribution could not be determined.

The normalized Si–OH and Si-OD responses from the in situ IR during the H_2 pulse into D_2 are shown in Fig. 5(b) for comparison with the deuterated propionaldehyde products. Comparing the H_2 and D_2 pulses, the Si–OH response was faster than the Si-OD response, suggesting an isotope effect on hydrogen spillover. The d_0-propionaldehyde and Si–OH decay responses are parallel, similar to the d_1- and d_2-propionaldehyde responses and Si-OD as shown in Fig. 2(b) and (c) and Fig. 3(b) and (c). The delay in the d_0-propionaldehyde second-hump response may be due to reaction with Si–OH.

5. Model development

The C_2H_5 ^{13}CHO response to the ^{13}CO pulse input results from (i) the reaction of $^*{}^{13}$CO with adsorbed $^*C_2H_5$ to form $^*C_2H_5$ ^{13}CO and (ii) the hydrogenation of $^*C_2H_5$ ^{13}CO to form $^*C_2H_5$ ^{13}CHO, as shown in the

following scheme:

$$E_{13} \longrightarrow \underset{\tau_{5CO}}{\boxed{{}^{*13}CO}} \xrightarrow{{}^{*}C_2H_5} \underset{\tau_{6CO}}{\boxed{{}^{*}C_2H_5^{13}CO}} \xrightarrow{{}^{*}H} E_{{}^{*}C_2H_5{}^{13}CHO,}$$

where E_{13CO} is the input pulse response. τ_{5CO} is the average surface residence time of the $^{*}CO$ before reaction with the $^{*}C_2H_5$ species to form $^{*}C_2H_5\ ^{13}CO$. τ_{6CO} is then the average surface residence time of $^{*}C_2H_5\ ^{13}CO$ before it is hydrogenated to form propionaldehyde. The lag of the $C_2H_5\ ^{13}CHO$ response behind the ^{13}CO response shown in Fig. 6 reflects the time required for ^{13}CO to travel through the reaction pathway to incorporate into the $C_2H_5\ ^{13}CHO$ product. The rate of transfer from ^{13}CO to $C_2H_5\ ^{13}CHO$ depends on the concentration of ^{13}CO, rate constant of the elementary steps, and the concentration of the corresponding reactants (i.e., $^{*}C_2H_5$, $^{*}H$) along the pathway [27].

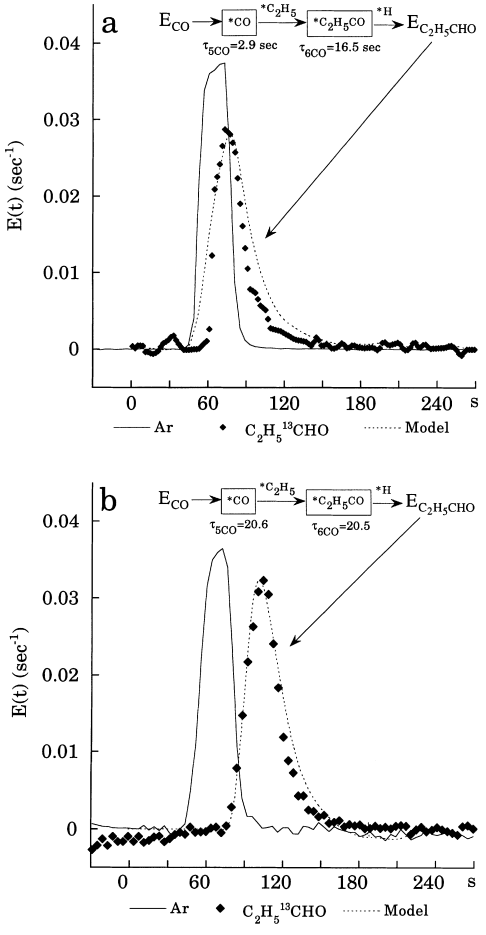

Fig. 6. Comparison of experimental $C_2H_5^{13}CHO$ response with compartment model response. The solid line is the input Ar response. The dashed line is the model result. (a) Rh/SiO_2 catalyst, and (b) $Mn–Rh/SiO_2$ catalyst. (Note that the Ar responses shown are the mirror images of the true responses.)

To simulate the transient $C_2H_5\ ^{13}CHO$ response, it is necessary to make a number of assumptions to reach a reasonable model with meaningful parameters. The following assumptions were used: (i) irreversible elementary steps for conversion of $^{*}CO$ to C_2H_5CHO and (ii) both the $^{*}C_2H_5CO$ and $^{*}C_2H_5CHO$ pools are lumped into a single pool with a single rate constant. The latter leads to a single value rate constant which may not be compatible with the heterogeneous catalyst surface. However, analysis of the propionaldehyde rate constant has shown that Rh/SiO_2 exhibited a single narrow rate constant distribution for propionaldehyde formation on Rh/SiO_2 [18]. Parallel ^{13}CO and $C_2H_5\ ^{13}CHO$ responses for the $Mn–Rh/SiO_2$ catalyst support uniform sites for propionaldehyde formation on $Mn–Rh/SiO_2$ [28]. Lumping of the steps allows analysis of the transient response with the original defined reaction pathway in Table 1 while significantly simplifying the simulation process and producing parameters with physical significance.

Applying a mole balance to the $^{*}CO$ and $^{*}C_2H_5CO$ pools results with

$$\tau_{5CO}\frac{dE_{^{*}CO}}{dt} + E_{^{*}CO} = E_{CO}, \tag{2}$$

$$\tau_{6CO}\frac{dE_{^{*}C_2H_5CO}}{dt} + E_{^{*}C_2H_5CO} = E_{^{*}CO}. \tag{3}$$

The computer program TUTSIM [29] was utilized to best fit the $C_2H_5\ ^{13}CHO$ experimental response to Eqs. (2) and (3) by varying τ_{5CO} and τ_{6CO}. Since $^{12}CO/Ar$ and ^{13}CO flowed over the catalyst with the same flow pattern, Ar was used as the input E_{CO}. The output of Eq. (2) was used as the input for Eq. (3), with $E_{C_2H_5CHO}$ being compared to the experimental $C_2H_5\ ^{13}CHO$ response. The best fit τ_{5CO} and τ_{6CO} are listed in Table 4(a). Interchanging the values between τ_{5CO} and τ_{6CO} results in the same transient response. Assigning the smaller value to τ_{5CO} for the Rh/SiO_2 results is consistent with the previous results of kinetic analysis suggesting that acyl hydrogenation is the rate limiting step for propionaldehyde formation [18,19]. Comparison of the best fit model responses (dashed

Table 4

Rh/SiO_2	$Mn–Rh/SiO_2$
(a) *Compartment modeling results and rate contant analysis for* ^{13}CO *and* H_2 *pulse*	
$E_{CO} \longrightarrow \boxed{*CO} \xrightarrow{*C_2H_5} \boxed{*C_2H_5CO} \xrightarrow{*H} E_{C_2H_5CHO}$	$E_{CO} \longrightarrow \boxed{*CO} \xrightarrow{*C_2H_5} \boxed{*C_2H_5CO} \xrightarrow{*H} E_{C_2H_5CHO}$
τ_{5CO}=2.9 s	τ_{5CO}=20.6 s
$TOF_{*C_2H_5CO}$=0.058 min^{-1}	$TOF_{*C_2H_5CO}$=0.32 min^{-1}
$TOF_{*C_2H_5CO} = \theta_{*CO}/\theta_{5CO}$	$TOF_{*C_2H_5CO} = \theta_{*CO}/\tau_{5CO}$
θ_{*CO}=0.003	θ_{*CO}=0.11
$TOF_{*C_2H_5CO} = k_{5CO}\theta_{*CO}\theta_{*C_2H_5}$	$TOF_{*C_2H_5CO} = k_{5CO}\theta_{*CO}\theta_{*C_2H_5}$
Because $\theta_{*C_2H_5}$ is unknown k_{5CO} cannot be calculated explicitly	Because $\theta_{*C_2H_5}$ is unknown k_{5CO} cannot be calculated explicitly
τ_{6CO}16.5 s	τ_{6CO}=20.5 s
TOF_{C_2CHO}=0.058 min^{-1}	$TOF_{C_2H_5CHO}$=0.32 min^{-1}
$TOF_{C_2H_5CHO} = \theta_{*C_2H_5CO}/\tau_{6CO}$	$TOF_{C_2H_5CHO} = \theta_{*C_2H_5CO}/\tau_{6CO}$
$\theta_{*C_2H_5CO}$=0.02	$\theta_{*C_2H_5CO}$=0.11
$TOF_{C_2H_5CHO} = k_{6CO}\theta_{*C_2H_5CO}\theta_{*H}$	$TOF_{*C_2H_5CHO} = k_{6CO}\theta_{C_2H_5CO}\theta_{*H}$
(θ_{*H}=0.10)	(θ_{*H}=0.14)
Thus k_{6CO}=36.4 min^{-1}	Thus k_{6CO}=20.9 min^{-1}
	$\boxed{*C_2H_4} \xrightarrow{*H} *C_2H_5 \xrightarrow{*CO} \boxed{*C_2H_5CO} \xrightarrow{Si\text{-}OH} E_{C_2H_5CHO}$
	τ_{5H}=0.5 s
	$TOF_{*C_2H_5CO}$ =0.16 min^{-1}
	$TOF_{*C_2H_5CO} = \theta_{*C_2H_5}/\tau_{5H}$
	$\theta_{*C_2H_5}$=0.03
	$TOF_{*C_2H_5CO} = k_{5H}\theta_{*C_2H_5}\theta_{*CO}$
	(θ_{*CO}=0.22)
	Thus k_{5H}=28.7 min^{-1}
	τ_{6H}=20.8 s
	$TOF_{C_2H_5CHO}$=0.16 min^{-1}
	$TOF_{C_2H_5CHO} = \theta_{*C_2H_5CO}/\tau_{6H}$
	$\theta_{*C_2H_5CO}$=0.05
	$TOF_{C_2H_5CHO} = k_{6H}\theta_{*C_2H_5CO}\theta_{*Si-OH}$
	Because θ_{*Si-OH} is unkown, k_{6H} cannot be calculated explicitly
Rh/SiO_2	$Mn–Rh/SiO_2$
(b) *Compartment modeling results and rate constant analysis for* D_2	
$E_{D_2} \longrightarrow \boxed{*C_2H_4} \xrightarrow{*H} *C_2H_5 \xrightarrow{*CO} \boxed{*C_2H_5CO} \xrightarrow{Si\text{-}OD} E_{C_2H_5CHO}$	$E_{D_2} \longrightarrow \boxed{*C_2H_4} \xrightarrow{*H} *C_2H_5 \xrightarrow{*CO} \boxed{*C_2H_5CO} \xrightarrow{Si\text{-}OD} E_{C_2H_5CHO}$
τ_{5D}=3.2 s	τ_{5D}=10.6 s
$TOF_{*C_2H_5CO}$=0.082 min^{-1}	$TOF_{*C_2H_5CO}$=0.16 min^{-1}
$TOF_{*C_2H_5CO} = \theta_{*C_2H_5}/\theta_{5D}$	$TOF_{*C_2H_5CO} = \theta_{*C_2H_5}/\tau_{5D}$
$\theta_{*C_2H_5}$=0.004	$\theta_{*C_2H_5}$=0.03
$TOF_{*C_2H_5CO} = k_{5D}\theta_{*C_2H_5}\theta_{*CO}$	$TOF_{*C_2H_5CO} = k_{5D}\theta_{*C_2H_5}\theta_{*CO}$
(θ_{*CO}=0.18)	(θ_{*CO}=0.22)
Thus k_{5D}=104 min^{-1}	Thus k_{5D}=25.0 min^{-1}
τ_{6D}=54.1 s	τ_{6D}=58.0 s
$TOF_{C_2H_5CDO}$=0.039 min^{-1}	$TOF_{C_2H_5CDO}$=0.040 min^{-1}
$TOF_{C_2H_5CDO} = \theta_{*C_2H_5CO}/\tau_{6D}$	$TOF_{C_2H_5CDO} = \theta_{*C_2H_5CO}/\tau_{6D}$
$\theta_{*C_2H_5CO}$=0.02	$\theta_{*C_2H_5CO}$=0.04
$TOF_{C_2H_5CDO} = k_{6D}\theta_{*C_2H_5CO}\theta_{*Si-OD}$	$TOF_{C_2H_5CDO} = k_{6D}\theta_{*C_2H_5CO}\theta_{*Si-OD}$
Because θ_{*Si-OD} is unkown k_{6D} cannot be calculated explicitly	Because θ_{*Si-OD} is unknown k_{6D} cannot be calculated explicitly

lines) and the experimental data (data points) is shown in Fig. 6.

The rate equations from these models can be written as follows [30]:

$$\mathrm{TOF}_{^*C_2H_5CO} = \frac{\theta_{^*CO}}{\tau_{5CO}}, \tag{4}$$

$$\mathrm{TOF}_{C_2H_5CHO} = \frac{\theta_{^*C_2H_5CO}}{\tau_{6CO}}. \tag{5}$$

Eqs. (4) and (5) were used to estimate the coverage of $^*CO$ and $^*C_2H_5CO$, respectively, and are presented in Table 4(a). According to the reaction scheme and mechanism listed in Table 1, the rate of adsorbed acyl and propionaldehyde formation can be described by

$$\mathrm{TOF}_{^*C_2H_5CO} = k_{5CO}\theta_{^*C_2H_5}\theta_{^*CO}, \tag{6}$$

$$\mathrm{TOF}_{C_2H_5CHO} = k_{6CO}\theta_{^*C_2H_5CO}\theta_{^*H}. \tag{7}$$

The elementary rate law for $^*C_2H_5CO$ and C_2H_5CHO formation consists of the product of adsorbate coverages assuming that these adsorbates ($^*CO$, $^*C_2H_5$, $^*C_2H_5CO$, and $^*H$) are well distributed on the catalyst surface.

Since $\mathrm{TOF}_{^*C_2H_5CO} = \mathrm{TOF}_{C_2H_5CHO}$ under steady-state conditions, equating the terms in Eqs. (4) and (6) results with

$$k_{5CO} = \frac{1}{\tau_{5CO}\theta_{^*C_2H_5}}. \tag{8}$$

Similarly, equating Eqs. (5) and (7) results with

$$k_{6CO} = \frac{1}{\tau_{6CO}\theta_{^*H}}. \tag{9}$$

Thus calculating the values of k_{5CO} and k_{6CO} requires information on $\theta_{^*C_2H_5}$ and $\theta_{^*H}$, respectively. An estimate of the $^*C_2H_5$ coverage is not available for either the Rh/SiO_2 or $Mn–Rh/SiO_2$ catalysts,therefore, k_{5CO} cannot be determined. Coverage of $^*H$ has been estimated for both the Rh/SiO_2 [23] and $Mn–Rh/SiO_2$ [20] catalysts from modeling of the H_2 pulse response during the D_2 pulse. The computed values of k_{6CO} are shown in Table 4(a).

The one-hump d_3-propionaldehyde response and the two-hump d_1- and d_2-propionaldehyde responses to the D_2 pulse in Fig. 3 shows the complexity of deuterium incorporation into these deuterated products. The first-hump of the d_1-propionaldehyde response has been suggested to result from H/D exchange on the adsorbed acyl species via keto-enol tautomerism and enol intermediates. The lack of information on the transient response of the $^*C_2H_5CO$ species during the D_2 pulse does not allow modeling of the first-hump response.

The compartment model describing the steps for d_0-propionaldehyde formation for the H_2 pulse in $CO/D_2/C_2H_4$ is shown by

$$E_{H_2} \longrightarrow \boxed{{}^*H \overset{{}^*C_2H_4}{\rightarrow} {}^*C_2H_5}_{\tau_{5H}} \overset{^*CO}{\rightarrow} \boxed{{}^*C_2H_5\,CO}_{\tau_{6H}} \overset{\text{Si-OH}}{\rightarrow} E_{C_2H_5CHO}$$

The parallel decay in the d_0-propionaldehyde and Si–OH responses to the H_2 pulse in Fig. 5 suggests the following reaction:

$$^*C_2H_5CO + \text{Si–OH} \rightarrow C_2H_5CHO + \text{Si–O} \tag{10}$$

Applying a mole balance to the $^*C_2H_5$ and $^*C_2H_5CO$ pools yields

$$\tau_{5H}\frac{dE_{^*C_2H_5}}{dt} + E_{^*C_2H_5} = E_{H_2}, \tag{11}$$

$$\tau_{6H}\frac{dE_{^*C_2H_5CO}}{dt} + E_{^*C_2H_5CO}E_{\text{Si–OH}} = E_{^*C_2H_5}. \tag{12}$$

Since H_2/Ar and D_2 flowed over the catalyst with the same flow pattern, Ar was used as the input E_{H_2} response. The $E_{^*C_2H_5}$ from Eq. (11) is utilized as the input for Eq. (12) and $E_{C_2H_5CHO}$ is the second hump of the d_0-propionaldehyde response. Table 4(a) contains the best fit and values while the best fit results are shown in Fig. 7 as the dashed lines. The assignment of the larger τ value to τ_{6H} is consistent with the slow decay of Si–OH on the catalyst. The model fits both the Rh/SiO_2 and $Mn–Rh/SiO_2$ catalysts supporting the previous modeling of the $C_2H_5\,{}^{13}CHO$ responses. Table 4(a) shows that k_{5H} can be computed from the rate law and known $\theta_{^*CO}$ from IR results. However, k_{6H} cannot be estimated because the coverage of *Si–OH is not available.

Similar fitting procedures were utilized to model the d_1-propionaldehyde and d_2-propionaldehyde second hump responses from the D_2 pulse. Fig. 8 shows the d_1-propionaldehyde fit for both catalysts. The TOF for d_1- and d_2-propionaldehyde was estimated by the area fraction of the second hump response as compared to all the deuterated propionaldehyde responses. The surface coverages of $\theta_{^*C_2H_5}$ and $\theta_{^*C_2H_5CO}$ and the corresponding rate constants are listed in Table 4(b).

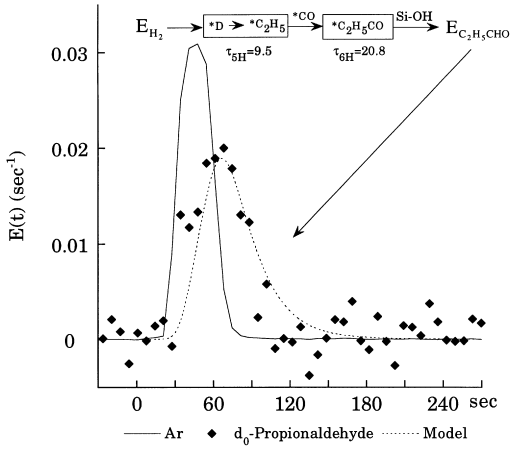

Fig. 7. Comparison of d_0-propionaldehyde second-hump model response with experimental data on Mn–Rh/SiO_2 catalyst. The solid line is the input Ar response. The dashed line is the model result.

Comparing the estimated surface coverages of the intermediate species during ethylene hydroformylation reveals differences in kinetic characteristics of the Rh/SiO_2 and Mn–Rh/SiO_2 catalysts. Estimates of the total CO coverage for both catalysts from previous IR studies suggest a similar coverage for adsorbed CO (0.18 for Rh/SiO_2 versus 0.22 for Mn–Rh/SiO_2). However, the adsorbed CO involved in propionaldehyde formation (see θ_{*CO} in Table 4(a) is vastly different for both catalysts. Coverages of adsorbed CO, ethyl, and acyl species are significantly higher on Mn–Rh/SiO_2 than Rh/SiO_2. The increase in the coverage of these active adsorbates on Mn–Rh/SiO_2 can be attributed to the increase in the active sites and the shift in the rate-limiting step. The former cannot be determined from this study; the latter is evidenced by the increase in τ_{5CO} from 2.9 to 20.6 s for the CO insertion step.

Both experimental determination and theoretical estimation of rate constants for elementary reactions remain in a rudimentary stage. Few rate constants of the elementary steps in steady-state heterogeneous catalytic reactions have been experimentally determined. These experimentally determined rate constants are needed for the verification of theoretical values of rate constants. Through an extensive effort, the steady-state isotopic transient studies have led to experimentally determined values of the elementary rate constants k_{5H} and k_{6CO} as shown in Table 4(a).

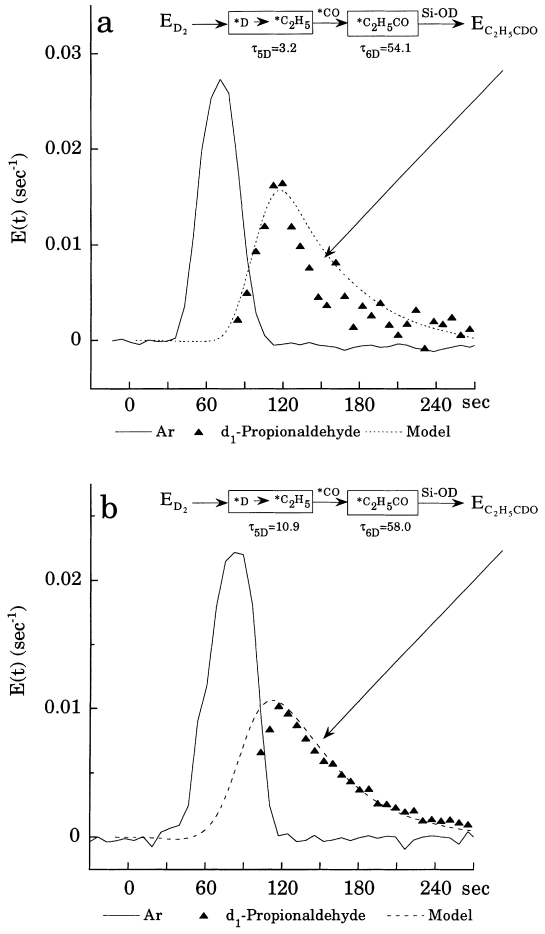

Fig. 8. Comparison of d_1-propionaldehyde second-hump model response with experimental data. The solid line is the input Ar response. The dashed line is the model result. (a) Rh/SiO_2 catalyst, and (b) Mn–Rh/SiO_2 catalyst. (Note that the Ar responses shown are the mirror images of the true responses.)

The use of transition state theory (TST) to estimate elementary rate constants requires knowledge of the partition functions of adsorbates and activated complexes as well as the activation energy of the elementary steps. The difficulty lies mostly in the estimation of the partition functions; however, there are some useful guidelines in the literature for determining values [31]. The elementary rate constant for acyl hydrogenation, k_m, may be calculated as follows:

$$k_m = \frac{k_b T}{h} \times \frac{Q_{AH}}{(Q_{*A})(Q_{*H})} \times \exp\frac{-E_a}{RT} \times \frac{\text{sites}}{\text{area}},$$

where k_b is the Boltzmann constant, h the Plank's constant, T the temperature in K, Q_{AH} the molecular partition function of the activated complex per unit area, Q_{*A} the molecular partition function of adsorbed acyl per unit area, Q_{*H} the molecular partition function of adsorbed hydrogen (on metal) per unit area, E_a the activation energy, and R is the gas constant. The activation energy was assumed to be 8.4 kcal mol^{-1} as an upper limiting value for acyl hydrogenation [18] while the sites per unit surface area were calculated as 1.963E13 cm^{-2} based on a support area of 350 m^2 g^{-1} and hydrogen chemisorption of 114 μmol g^{-1} for Mn–Rh/SiO_2 [22]. The factor sites/area is a factor that arises from the conversion of rate and surface concentration to TOF and coverage. Q_{AH} was assumed to be an immobile species with one degree of rotational freedom, Q_{*A} a mobile species with three degrees of rotational freedom, and Q_{*H} a mobile species with one degree of rotational freedom, yielding values of 1E16, 2.5E20, and 2.5E18 cm^{-2}, respectively. Plugging these values into the TST yields a value of 52.5 min^{-1} for acyl hydrogenation. This is in the same order of magnitude with k_{6CO} for Rh/SiO_2 and Mn–Rh/SiO_2, 36.4 and 20.9 min^{-1}, respectively.

6. Conclusions

The formation of propionaldehyde from syngas and ethylene involves half hydrogenation of adsorbed ethylene to form an adsorbed ethyl species, the insertion of adsorbed CO into the ethyl species to produce an adsorbed acyl species, and the hydrogenation of this acyl species to form propionaldehyde. A pulse injection of D_2 into H_2 with CO and C_2H_4 over Rh/SiO_2 and Mn–Rh/SiO_2 yielded two-hump responses for both d_1- and d_2-propionaldehyde and a single-hump response for d_3-propionaldehyde. The two-hump responses are the result of different isomers produced by different deuterium pathways. Further pulse experiments have suggested that (i) the first hump is produced from rapid H/D exchange with adsorbed propionaldehyde via enol intermediates and (ii) the decay of the second hump is due to reaction of adsorbed acyl with Si–OH/Si-OD, spillover hydrogen/deuterium, respectively.

Compartment modeling of the transient responses have allowed determination of residence times of adsorbed intermediates, surface coverages of adsorbed intermediates, and the elementary rate constants for acyl hydrogenation and CO insertion. The elementary rate constants of acyl hydrogenation on Rh/SiO_2 and Mn–Rh/SiO_2 were compared to the value estimated from transition state theory and were found to be within the same order of magnitude.

Compartment modeling of transient responses revealed that addition of Mn promoter to Rh/SiO_2 increased coverages of $^*CO$, $^*C_2H_5$, and $^*C_2H_5CO$ and shifted the rate-limiting step for propionaldehyde formation. Acyl hydrogenation is the rate-limiting step on Rh/SiO_2 while CO insertion and acyl hydrogenation are kinetically significant on Mn–Rh/SiO_2.

Acknowledgements

The authors gratefully acknowledge the partial support of this research by the National Science Foundation under grant CTS-9421119996.

References

[1] O. Levenspiel, Chemical Reaction Engineering, 2nd ed., Wiley, New York, 1972.
[2] C. Wen, L. Fan, Models for Flow Systems and Chemical Reactors, Marcel Dekker, New York, 1975.
[3] G. Stephanopoulos, Chemical Process Control: An Introduction to Theory and Practice, Prentice-Hall, Englewood Cliffs, 1992.
[4] W. Luyben, Process Modeling, Simulation, and Control for Chemical Engineers, McGraw-Hill, New York, 1990.
[5] D. Coughanowr, Process Systems Analysis and Control, 2nd ed., McGraw-Hill, New York, 1991.
[6] G. Froment, K. Bischoff, Chemical Reactor Analysis and Design, Wiley, New York, 1979.
[7] H.S. Fogler, Elements of Chemical Reaction Engineering, Prentice-Hall, Englewood Cliffs, 1992.
[8] G. Parravano, Catal. Rev. 3 (1969) 207.
[9] A.M. Efstathiou, C.O. Bennett, J. Catal. 120 (1989) 137.
[10] N.W. Cant, A.T. Bell, J. Catal. 73 (1982) 257.
[11] P. Biloen, J.N. Helle, F.G.A. van den Berg, W.M.H. Sachtler, J. Catal. 81 (1983) 450.
[12] T. Koerts, R. van Santen, J. Catal. 134 (1992) 13.
[13] J. Nwalor, J.G. Goodwin Jr, P. Biloen, J. Catal. 117 (1989) 121.
[14] J. Happel, S. Kiang, J.L. Spencer, S. Oki, M.A. Hnatow, J. Catal. 50 (1977) 429.
[15] C. Mirodatos, J. Phys. Chem. 90 (1986) 481.
[16] S. Shannon, J.G. Goodwin Jr., , Chem. Rev. 95 (1995) 677.
[17] P. Emmett, Catal. Rev. 7 (1972) 1.

[18] M.W. Balakos, S.S.C. Chuang, J. Catal. 151 (1995) 253.
[19] M.W. Balakos, S.S.C. Chuang, J. Catal. 151 (1995) 266.
[20] M.A. Brundage, Dynamic Isotopic Modeling of Ethylene Hydrogenation and Hydroformylation Over Metal Catalysts, Ph.D. Dissertation, The University of Akron, 1997.
[21] S.S.C. Chuang, M.A. Brundage, M.W. Balakos, G. Srinivas, Appl. Spectr. 49 (1995) 1151.
[22] M.A. Brundage, S.S.C. Chuang, J. Catal. 174 (1998) 164.
[23] M.A. Brundage, S.S.C. Chuang, J. Catal. 164 (1996) 94.
[24] T. Mazanec, J. Catal. 98 (1986) 115.
[25] A. Takeuchi, J.R. Katzer, J. Phys. Chem. 86 (1982) 2438.
[26] J. Horiuti, M. Polanyi, Trans. Faraday Soc. 30 (1934) 1164.
[27] J. Happel, Isotopic Assessment of Heterogeneous Catalysis, Academic Press, New York, 1986.
[28] S.S.C. Chuang, M.A. Brundage, M.W. Balakos, Appl. Catal. A 151 (1997) 333.
[29] W. Reynolde, J. Wolf, TUTSIM Block Diagram Language, TUTSIM Products, Palo Alto, CA, 1991.
[30] P. Biloen, J. Mol. Catal. 21 (1983) 17.
[31] J.A. Dumesic, D.F. Rudd, L.M. Aparicio, J.E. Rekoske, A.A. Trevino, The Microkinetics of Heterogeneous Catalysis, American Chemical Society, Washington, DC, 1993.